

Pluto Photometry Conversion Independent Study

TIM EWING¹

¹ University of Colorado, Boulder

1. INTRODUCTION

The goal of this independent study is to convert observations using the MVIC (Multispectral Visible Imaging Camera) instrument on the New Horizons spacecraft to the filter set on the Hubble Space Telescope in order to compare the New Horizons data to existing Hubble Space Telescope data. Since the filters on MVIC do not match those on HST, conversion between the systems is needed. We transform observations of Pluto and Charon with the Red and Blue filters into the HST F555W and F435W filters in order to compare them to observations made in Buie 2010. Conversion of the observations involves compensation for the varying distance of the target from the sun and the spacecraft as well as performing synthetic observations by integrating the convolution of the target spectrum and the passband of the filter. Some of these calculations are performed using Pysynphot, but others must be performed by hand. The transformations were performed for the HST F555W and F435 filters for observations of Pluto and Charon, as well as for a standard solar-type star (HD-205905).

2. OBSERVATIONS

Visible-wavelength color observations on New Horizons are accomplished with the Multi-Spectral Visible Imaging Camera (MVIC) component of the Ralph instrument. MVIC has seven detectors at its focal plane: 6 time delay integration (TDI) CCDs and one panchromatic frame transfer CCD. Two of the TDI arrays are panchromatic providing a wide field of view, 5.7 degrees orthogonal to the scan direction needed to build up the charge for time delay integration. The remaining 4 TDI arrays provide the multi-spectral capability with 3 broadband channels and one narrow band channel designed to detect methane ice on Pluto's surface. An in-depth description and derivation of the responsivity curves for the MVIC filters is given in Howett et al. 2017 (p140). Although these filters cover a similar range of wavelengths as those of the HST F555W and F435 filters, they do not line up one-to-one; Figure 2.1 shows a comparison of the MVIC red and blue filter throughputs with those of the comparable HST ACS filters. Data for this project were obtained from the New Horizons Science Operations Center and from the included resources in the Python Pysynphot package (STScI Development Team (2013)).

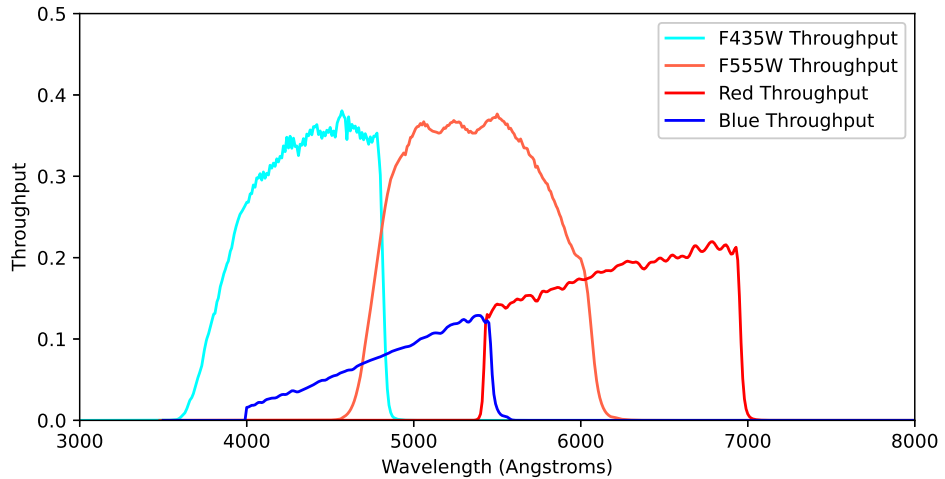


Figure 2.1. Select filter passbands for MVIC (Red and Blue) on New Horizons and ACS (F435W and F555W) on the Hubble Space Telescope.

3. FIRST SEMESTER

3.1. Single-filter Conversion

Since the MVIC and ACS passbands differ, transformation between the two systems is more complicated than simply scaling the flux according to the different distances. Instead, a best guess at the spectrum observed by the output observatory must be generated in order to perform a synthetic observation. Derivation of this spectrum is a multi-step process. This paper takes New Horizons as the input, HST as the output, and Pluto (or occasionally Charon) as the target; however, the method is fully general and can be used for any observatories and target given a known spectrum and passbands.¹

First, the known spectrum of Pluto is multiplied by a scalar in order to correct the magnitude to match that of the observation:

$$F_{NH}(\lambda) = F_{\mathbb{P}}(\lambda) * \frac{F_{obs}}{F_{\mathbb{P}}(\lambda_P)} \quad (1)$$

Where $F_{NH}(\lambda)$ is the spectrum observed by New Horizons, $F_{\mathbb{P}}(\lambda)$ is the spectrum global of Pluto, F_{obs} is the observed flux at the pivot wavelength, and $F_{\mathbb{P}}(\lambda_P)$ is the flux of the global spectrum of Pluto evaluated at the pivot wavelength, λ_P . Then, the input spectrum $F_{in}(\lambda)$ is multiplied by another pair of scalars. One compensates for the differing distance from the observatories to Pluto, and the other for the differing distance from Pluto to the sun:

$$F_{HST}(\lambda) = F_{NH}(\lambda) * \left[\frac{R_{\mathbb{P}}(NH)}{R_{\mathbb{P}}(HST)} \right]^2 * \left[\frac{R_{NH}}{R_{HST}} \right]^2 \quad (2)$$

Where $F_{HST}(\lambda)$ is the approximation of the spectrum observed by the HST ACS, $R_{\mathbb{P}}(NH)$ and $R_{\mathbb{P}}(HST)$ refer to the distance from Pluto to the Sun, and R_{NH} and R_{HST} refer to the distance from the respective observatory to Pluto for each observation. For this paper, however, $R_{\mathbb{P}}(HST) = 39.5AU$ and $R_{HST} = 38.5AU$ for all of the HST observations to match the existing data in Buie et al. (2010). Finally, the synthetic observation is performed by integrating the convolution of the spectrum observed $F_{HST}(\lambda)$ by the throughput of the HST ACS F555W or F435 filter over all wavelengths:

$$F_{HST}(\lambda) = \int F_{HST}(\lambda) \cdot T(\lambda) d\lambda \quad (3)$$

Where $T(\lambda)$ is the system throughput of the HST ACS filter as a function of wavelength. The result of 3 is the Vegamag of a single observation converted from the New Horizons filters to the HST ACS F555W or F435W.

3.2. Multi-filter Conversion

Table 1. Conversion Weights

Target Input Filter	Pluto		Charon		HD205905	
	Red	Blue	Red	Blue	Red	Blue
F555W	0.5479	0.4521	0.5237	0.4763	0.5388	0.4612
F435W		1.0000		1.0000		1.0000
Johnson V	0.5830	0.4170	0.5638	0.4362	0.5781	0.4219
Johnson B	0.0069	0.9931	0.0055	0.9945	0.0061	0.9939
Johnson R	0.9913	0.0087	0.9905	0.0095	0.9915	0.0085

For some desired transformations, more than one input passband overlap with the output passband. In these instances, a method for conversion from both filters is possible. In this paper, this is accomplished by combining the results of the single-filter conversions using a weighted average based on the overlap of the input passband with the

¹ All calculations here use flux in units of Flam ($erg \cdot s^{-1} \cdot cm^{-2} \cdot \text{\AA}^{-1}$). Use of a nonlinear unit like Absolute Magnitude or Vegamag with these equations will produce erroneous results.

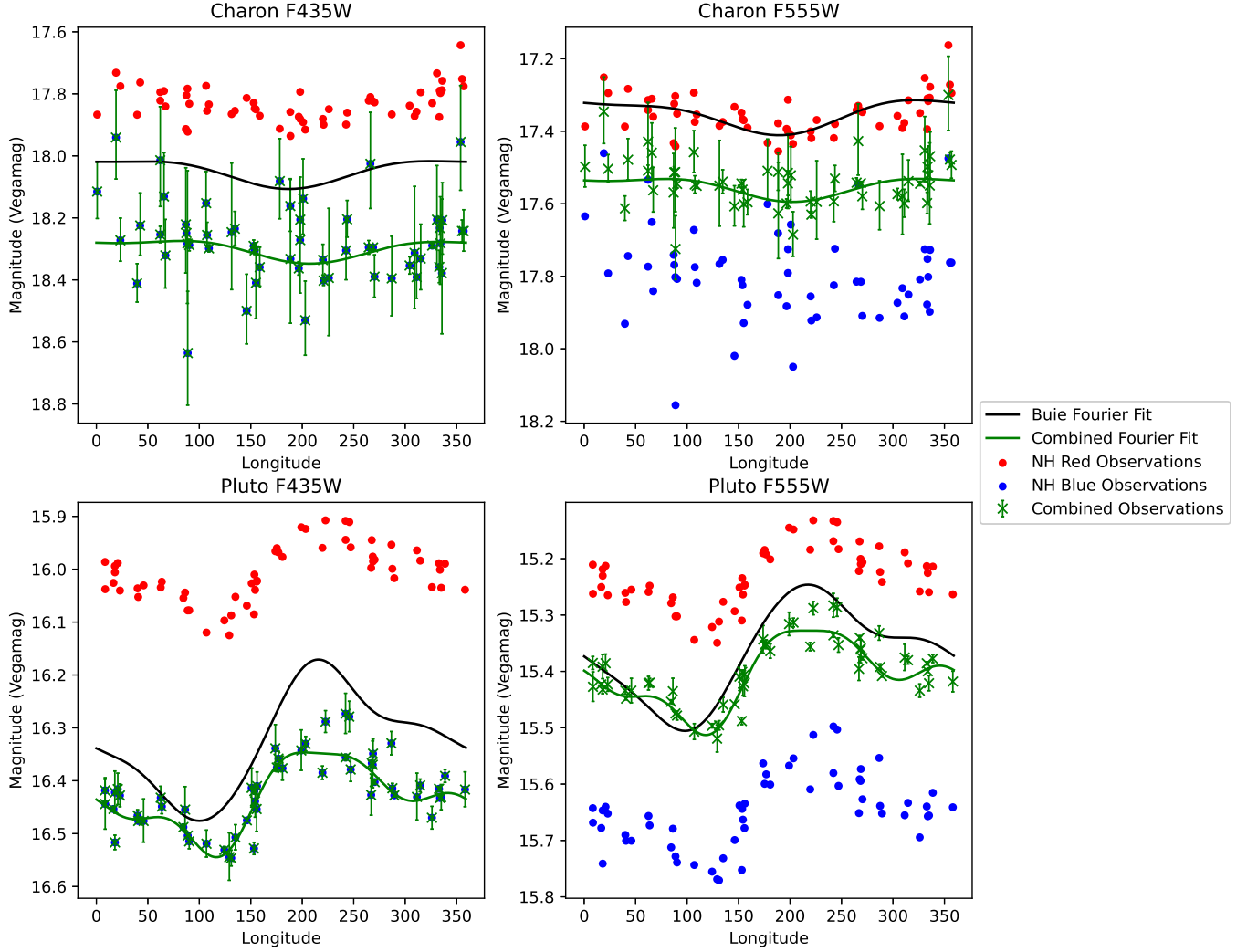


Figure 3.1. Rotational light curves for Pluto and Charon in the F435W and F555W filters. [Tim: note these are rotational light curves because it is flux as it rotated. Phase curves are curves as a function of solar phase angle The red and blue points are the converted values from the NH Red and NH Blue filters respectively. The green crosses with error bars are the converted values using the combined NH Red and NH Blue values. The black curve is the Fourier series fit from (Buie et al. 2010). The green curve is the least-squares Fourier fit to the New Horizons data (green points) with coefficients shown in Tables 3, 4, 5, and 6. The Fourier fit to the data is the same order used by (Buie et al. 2010)]

output passband in the context of the target spectrum. A list of the relative contributions for select inputs, outputs, and targets is listed in Table 1, calculated according to Eq. 4.

It should be noted that for conversions to the HST F435W filter, the combined result and the Blue result are identical. Since the NH Red filter overlaps almost none with the HST F435 filter, this result is expected because the weighting on the Red filter is almost zero. However, the conversion process should still result in a similar answer for the Red filter as for the Blue filter. Since the New Horizons Red filter gives transformed magnitudes approximately 0.3 Magnitudes higher than the existing data for Pluto and Charon, there is likely an issue in the process. One possible source for the 0.3 mag difference is the assumed Pluto spectra used in the transformation. This work is using the standard New Horizons Pluto spectrum which is based on ground-based observations.

$$C_i = \frac{\int F_P(\lambda) \cdot T_i(\lambda) \cdot T_{out}(\lambda) d\lambda}{\sum_j \int F_P(\lambda) \cdot T_j(\lambda) \cdot T_{out}(\lambda) d\lambda} \quad (4)$$

The method of transformation for these filters was also verified using a standard star, HD-205905. The results of the comparison are in Table 2. These transformation shows that the method is accurate to ± 0.1 Vegamag.

We find that the result of conversions for HD-205905 does not differ greatly between the Red, Blue, and Combined input filters. This is the expected result and works for the HD-205905 data. This observation is a well-known solar analog and a solar spectrum was used for the transformation.

Table 2. HD-205905 transformation with comparison to SIMBAD. These results show that the transformations are accurate to ± 0.1 Vegamag.

Output Filter	Conversion	Result	SIMBAD Result
		(Vegamag)	(Vegamag)
F555W	Red	6.65	6.74
F555W	Blue	6.64	6.74
F555W	Combined	6.65	6.74
F435W	Red	7.25	7.36
F435W	Blue	7.24	7.36
F435W	Combined	7.24	7.36

4. SECOND SEMESTER

4.1. Error Analysis

An important part of understanding this data is understanding the error of each datapoint. The error of the data is roughly proportional to the distance from Pluto at which the data was taken, so there is significant variation throughout the dataset. Propagating error through a process like this is often a cumbersome process. However, since each of the steps involved is one-to-one, it is instead possible to simply rerun the full conversion with the upper and lower bounds added to the datapoint. The results of this process are included in Figure 3.1. The error bars are only shown for the combined fit data because these are the preferred results from the conversion to HST passbands. For the F435W transformation, the results from the NH Blue filter and the Combined method are nearly identical, so either could be used.

4.2. Fourier Fit

Buie et al. (2010) uses a 5- or 3-term Fourier series fit for Pluto and Charon respectively to describe the phase curve of the targets. In order to compare the new conversions to the existing data, we use a least-squares Fourier series fit with the same number of terms to fit the new data. The Fourier fits are included as the green curve in Figure 3.1 and the coefficients are included in Tables 3, 4, 5, and 6.

4.3. Historical Comparison

With the errors calculated and the Fourier series fit applied, we are now ready to make comparisons to previous datasets. Buie et al. (2010) took data using the HST Advanced Camera for Surveys with the F435W and F555W filters in 2002. These data were taken at phase angles of less than 1.74° and were normalized to account for the opposition spike. In contrast, the data presented in this paper were taken at phase angles of 14.50° to 15.06° . Figure 3.1 shows the Fourier series fit from Buie et al. (2010) in black and the fit from this paper in green. The difference of the New Horizons' data and Fourier fit to the HST data is shown in Figure 3.2. The black datapoints show the converted observations from 3.1 minus the Buie Fourier fit at that sub-observer longitude; the red curve is the difference between the two Fourier curves (the New Horizons Fourier fit minus the HST Fourier fit from Buie et al. (2010)). We find that the difference of fits is mostly longitude-independent for Charon, with the difference being approximately 0.25 magnitudes for the F435W filter and 0.2 magnitudes for the F555W filter. For Pluto, however, we find significant dependence in magnitude on longitude. In both the F435W and F555W filters, the area around $50^\circ - 100^\circ$ longitude

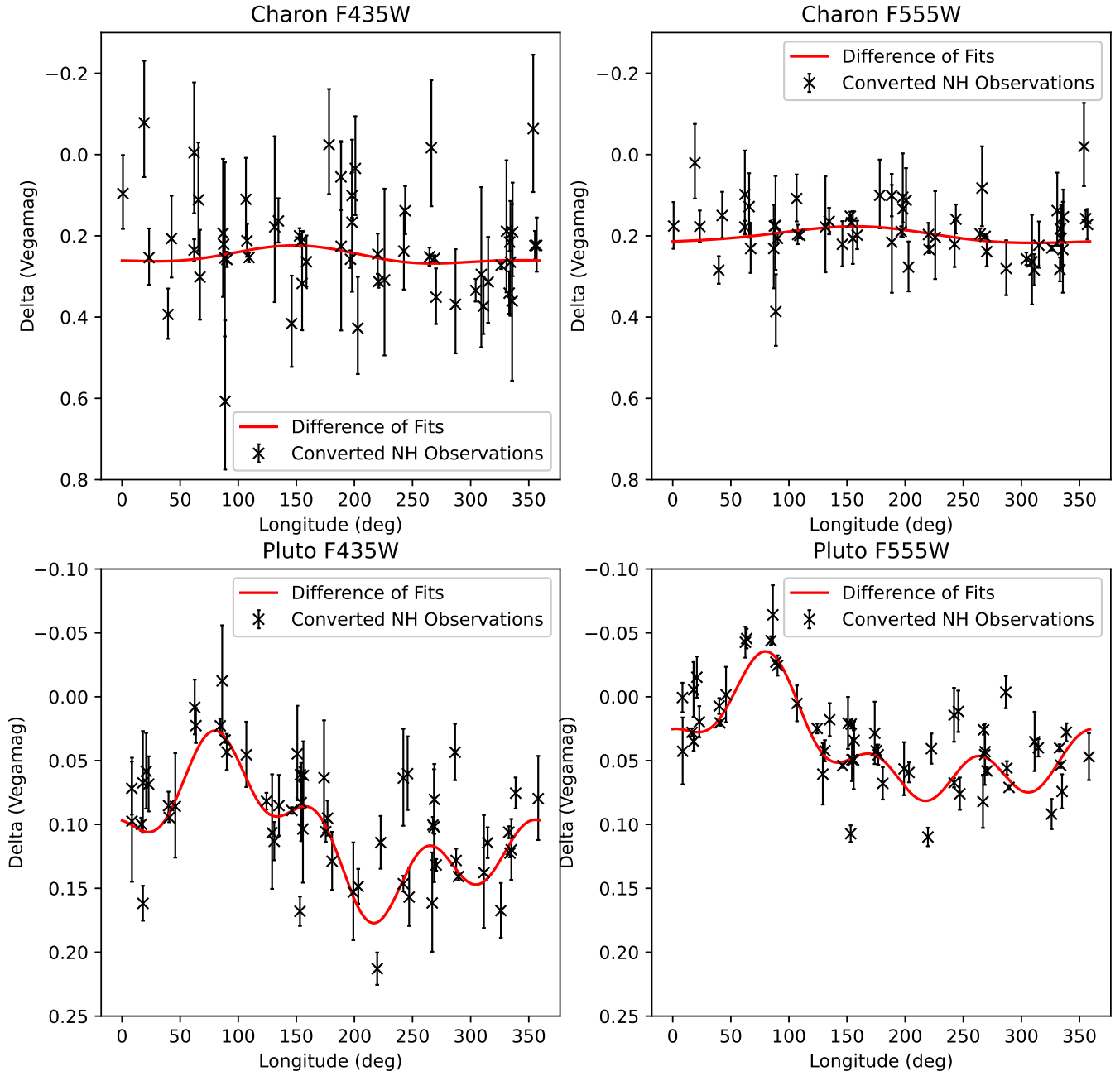


Figure 3.2. Differences between the converted NH Magnitudes and the Fourier series fit from (Buie et al. 2010) The black crosses are the converted magnitude minus the magnitude of Buie's fit at that longitude. The red line is the NH Fourier fit from Tables 3, 4, 5, and 6 minus the fit from (Buie et al. 2010).

is relatively brightened. The difference in fits varies from approximately 0.2 to 0.17 magnitudes for the F435W filter, and from approximately -0.04 to 0.07 magnitudes for the F555W filter.

A comparison to literature shows that the differences in magnitude for Charon could potentially be explained by the differing phase angle. Figure 4.1 shows the phase curve of different Kuiper Belt objects. The difference in magnitudes for these objects is approximately 0.5-1.0 magnitudes from 1° to 15° . Although Charon and Cyrene are very different bodies, this shows that deltas of 0.2-0.25 magnitudes are reasonable.

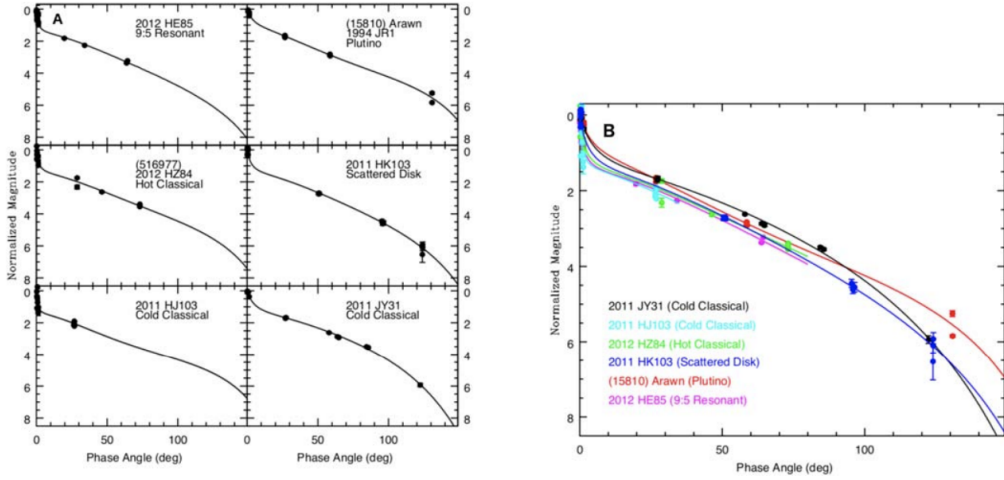


Figure 4.1. From Verbiscer et al. (2019) the phase function for different Kuiper Belt Objects.

Table 3. Least Squares Fourier Series fit terms for Charon in the F435W passband.

n	a _n	b _n
0	18.29990	0.0
1	-0.02897	-0.01622
2	0.00907	0.01160

Table 4. Least Squares Fourier Series fit terms for Charon in the F555W passband.

n	a _n	b _n
0	17.55258	0.0
1	-0.02672	-0.01072
2	0.00968	0.00947

The differences of magnitude for Pluto are less easily explained. The total deltas are within reason for simple phase angle variation, but the strong longitude dependence requires an alternative explanation. Pluto shows more variation in the reflectivity and color of the surface than Charon, so the longitude dependence could be explained by a difference in visible terrain between the two datasets; testing this theory is outside the scope of this project.

The conversion from New Horizons filter sets to the HST filter sets used a global spectrum for Pluto. Motivated by the variation in the color of Pluto's surface features, I next performed an analysis of the sensitivity of the conversion method to spectral differences.

Table 5. Least Squares Fourier Series fit terms for Pluto in the F435W passband.

n	a _n	b _n
0	16.43281	0.0
1	0.02623	0.06480
2	-0.02386	-0.03283
3	0.01081	0.00662
4	-0.01046	0.01299

Table 6. Least Squares Fourier Series fit terms for Pluto in the F555W passband.

n	a _n	b _n
0	15.40760	0.0
1	0.01962	0.06159
2	-0.02342	-0.03252
3	0.00614	0.00786
4	-0.01126	0.01147

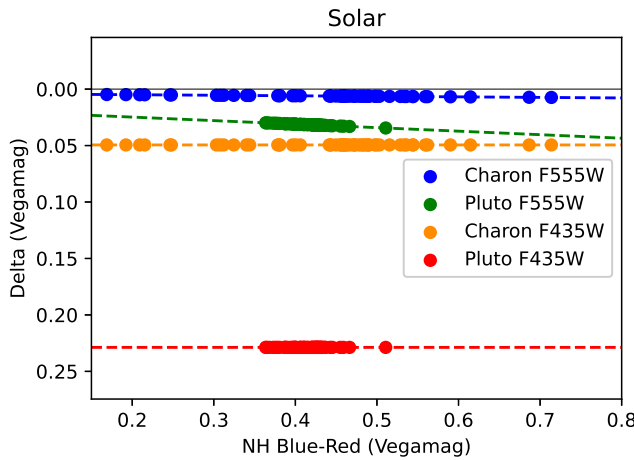


Figure 4.2. Difference in converted magnitude using the Solar spectrum instead of the Pluto/Charon spectra. The x-axis is the converted NH Blue magnitude minus the converted NH Red magnitude. The dotted lines are the lines of best fit.

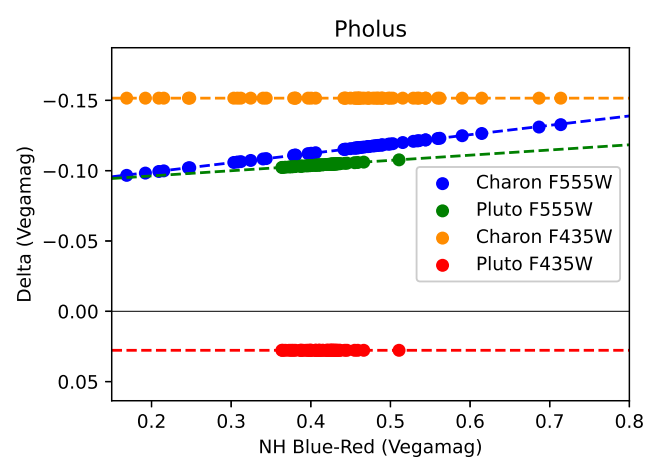


Figure 4.3. Difference in converted magnitude using the Pholus spectrum instead of the Pluto/Charon spectra. The x-axis is the converted NH Blue magnitude minus the converted NH Red magnitude. The dotted lines are the lines of best fit.

4.4. Sensitivity Analysis

Two alternative spectra were selected in order to characterize the sensitivity of the conversion method to spectral differences: Pholus and the Sun. These two spectra were selected to bracket the visible surface features on Pluto: Pholus is more red than Pluto and the Sun more blue. The spectra, normalized to have a Vegamag of 0 when convolved over the NH Blue passband, are shown in Figure ???. Note that the Pholus flux is higher in the area spanned by the NH Red passband and the Solar flux is lower in the same region. Figure ?? shows the same plot normalized to the Pluto flux in order to better represent the differences.

The full conversion process was run for both targets and both filters using the Solar and Pholus spectra. A version of Figure 3.1 for the Pholus and Solar spectra is included in the appendix.

Figure 4.2 shows the differences using the Solar spectrum with the NH Red and NH Blue throughputs included for context. The lines of best fit have equations $0.0000x + 0.0494$ for Charon F435W, $0.0000x + 0.2288$ for Pluto F435W, $0.0048x + 0.0040$ for Charon F555W, and $0.0312x + 0.0186$ for Pluto F555W. Since the Solar spectrum is close to the Charon spectrum, the differences for the two Charon datasets are within 0.05 Vegamag. For Pluto, the difference between the Pluto spectrum and the Solar spectrum is much more significant. For the F555W conversion, the decrease in the NH Blue convolved flux is mostly offset by the increase in the NH Red convolved flux so the overall difference is small. For the Pluto F435W conversion, only the NH Blue filter is used and the overall delta is much higher.

Figure 4.3 shows the differences using the Pholus spectrum with the NH Red and NH Blue passbands included for context. The lines of best fit have equations $0.0000x - 0.1516$ for Charon F435W, $0.0000x + 0.0277$ for Pluto F435W, $-0.0665x - 0.0857$ for Charon F555W, and $-0.0369x - 0.0889$ for Pluto F555W. Since Pholus is much redder than Pluto and Charon, both F555W conversions end up significantly brightened. The Pholus spectrum matches the Pluto spectrum well in the 3000-5500 Angstrom region, so the Pluto F435W spectrum is mostly unaffected. The Charon spectrum has higher, decreasing flux in the 3000-5500 Angstrom region compared to the Pholus spectrum, so the Charon F435W conversion is brightened.

5. FUTURE WORK

The next step in this project is to more scientifically determine if the difference from Buie et al. (2010) can be explained by the differing viewing geometry. Since Pluto varies significantly in color and albedo across the surface, it is possible the longitude dependence of the differences can be explained simply by differences in visible geometry. This comparison is a nontrivial task, however, and is outside the scope of this semester.

6. CONCLUSIONS

We find that observations using New Horizons Red and Blue filters can be compared to those made using the HST F435W and F555W filters. We find that the NH Blue filter is sufficient to transform to the HST F435W filter, but that a combination of both the Red and the Blue filters is required to accurately transform to the HST F555W filter. After transformation, the difference in phase curves on Charon is estimated to be approximately 0.25 magnitudes for the F435W filter and 0.2 magnitudes for the F555W filter. On Pluto, we find significant sub-observer longitude variation in differences with values between approximately 0.2 to 0.17 magnitudes for the F435W filter, and from approximately -0.04 to 0.07 magnitudes for the F555W filter.

ACKNOWLEDGMENTS

Over the last two semesters, I have written over 1600 lines of Python and made significant advances in my understanding of optics and data analysis. This project has taught me new branches of Physics and has helped prepare me for writing more robust scientific data pipelines in the future. I'd like to thank Cathy Olkin and John Keller for making it possible.

Facilities: HST(STIS)

Software: astropy (Astropy Collaboration et al. 2013), pysynphot (STScI Development Team 2013),

REFERENCES

- Astropy Collaboration, Robitaille, T. P., Tollerud, E. J., et al. 2013, A&A, 558, A33, doi: [10.1051/0004-6361/201322068](https://doi.org/10.1051/0004-6361/201322068)
- Buie, M. W., Grundy, W. M., Young, E. F., Young, L. A., & Stern, S. A. 2010, The Astronomical Journal, 139, 1117, doi: [10.1088/0004-6256/139/3/1117](https://doi.org/10.1088/0004-6256/139/3/1117)
- STScI Development Team. 2013, pysynphot: Synthetic photometry software package. <http://ascl.net/1303.023>

APPENDIX

A. ADDITIONAL FIGURES

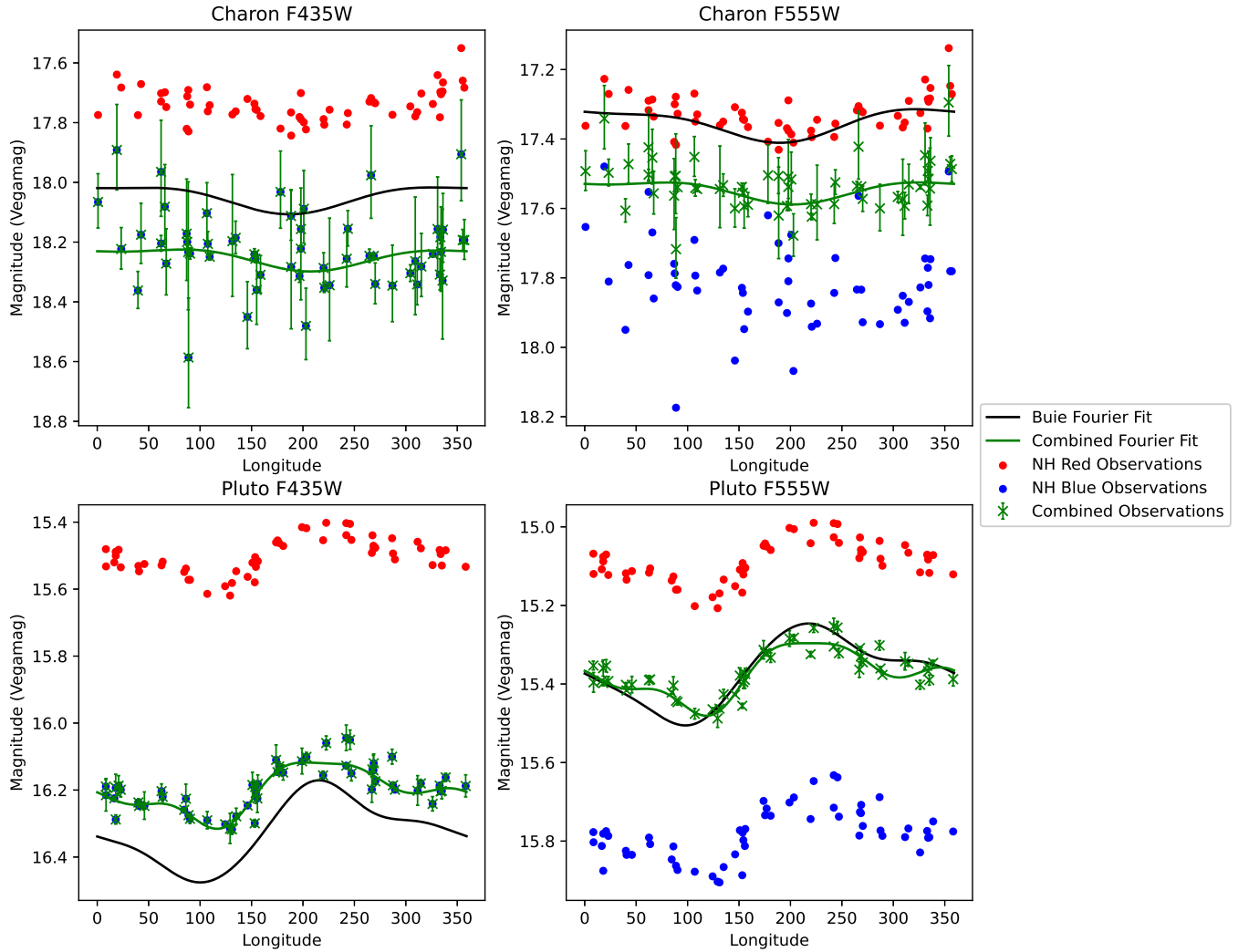


Figure A.1. A copy of Figure 3.1 computed using the Solar spectrum.

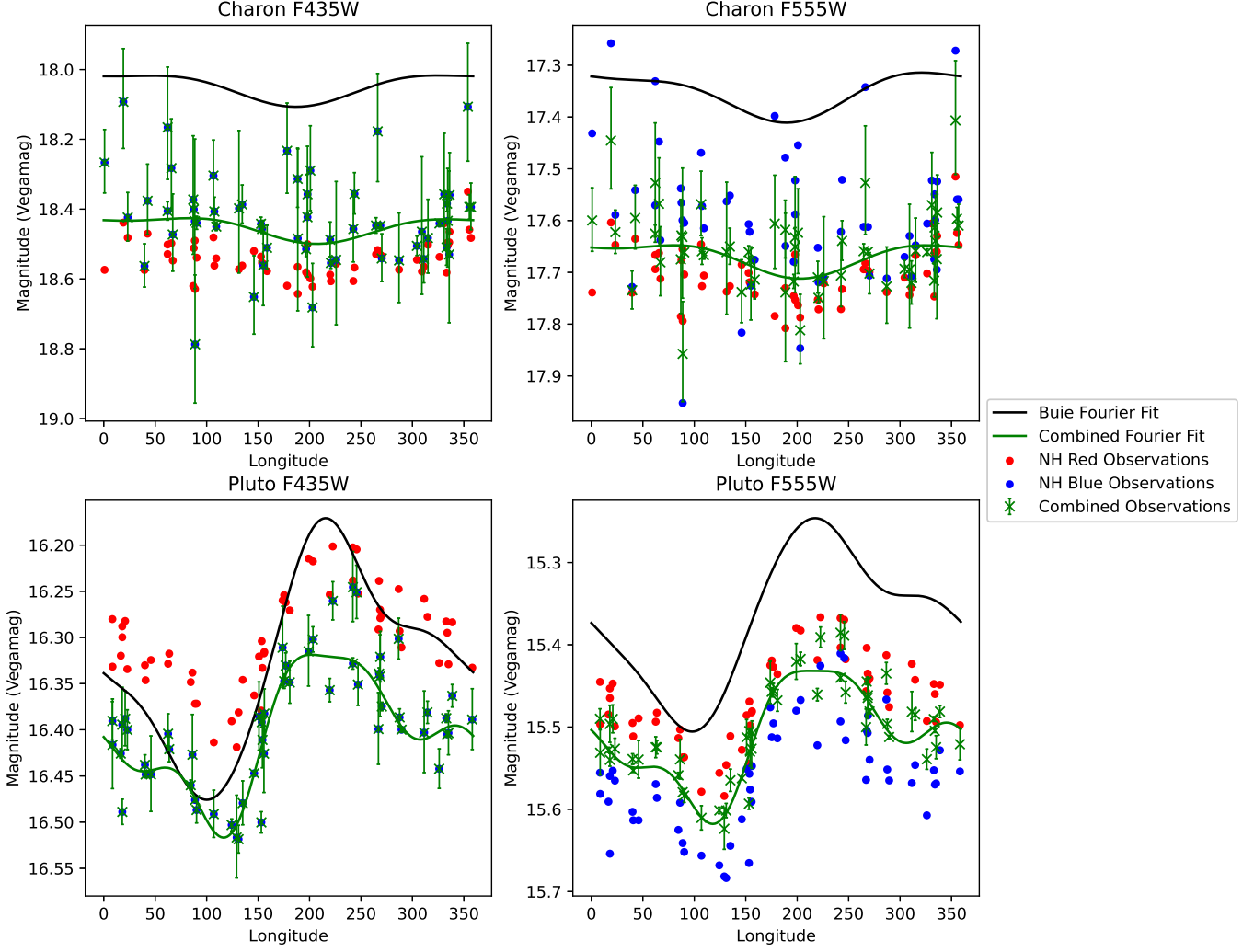


Figure A.2. A copy of Figure 3.1 computed using the Pholus spectrum.

B. SOURCE DATA: PLUTO/CHARON OBSERVATIONS

[h]

Table 7. Color Observations of Pluto

	Mid-Time of Observation (UTC)	MET	Image Scale (km/pix)	Sub-s/c Long. (Deg E)	Sub-s/c Lat. (Deg N)	Solar Phase. (Deg)	Electronics
APMV_PC_COLOR_099_SCI1	2015-04-09T04:49:05.341	290860857	2294	174	43	14.5	0
APMV_PC_COLOR_102_SCI1	2015-04-12T03:12:05.344	291114237	2224	9	43	14.5	1
APMV_PC_COLOR_103_SCI1	2015-04-13T03:32:05.346	291201837	2200	311	43	14.5	0
APMV_PC_COLOR_103_SCI3	2015-04-13T21:48:05.346	291267597	2181	269	43	14.5	1
APMV_PC_COLOR_104_SCI1	2015-04-14T09:03:05.347	291308097	2170	242	43	14.5	0
APMV_PC_COLOR_105_SCI1	2015-04-15T03:22:05.348	291374037	2152	199	43	14.5	1
APMV_PC_COLOR_105_SCI3	2015-04-15T21:50:05.348	291440517	2134	156	43	14.5	0
APMV_PC_COLOR_106_SCI1	2015-04-16T09:08:05.349	291481197	2123	129	43	14.5	1
APMV_PC_COLOR_107_SCI1	2015-04-17T03:26:05.350	291547077	2104	86	43	14.5	0

Table 7 continued on next page

Table 7 (*continued*)

	Mid-Time of Observation	MET	Image Scale	Sub-s/c Long.	Sub-s/c Lat.	Solar Phase.	Electronics
	(UTC)		(km/pix)	(Deg E)	(Deg N)	(Deg)	Side
APMV_PC_COLOR_107_SCI3	2015-04-17T20:36:05.350	291608877	2087	46	43	14.5	1
APMV_PC_COLOR_108_SCI1	2015-04-18T08:29:05.351	291651657	2076	18	43	14.5	0
APMV_PC_COLOR_110_SCI1	2015-04-20T07:45:05.353	291821817	2029	267	43	14.6	1
APMV_PC_COLOR_112_SCI1	2015-04-22T09:11:05.355	291999777	1980	151	43	14.6	0
APMV_PC_COLOR_117_SCI1	2015-04-27T02:04:05.360	292406157	1868	246	43	14.6	0
APMV_PC_COLOR_118_SCI1	2015-04-28T17:02:05.362	292546437	1829	154	43	14.6	1
APMV_PC_COLOR_121_SCI1	2015-05-01T01:51:05.364	292750977	1773	21	43	14.6	0
APMV_PC_COLOR_123_SCI1	2015-05-03T01:33:35.366	292922727	1725	269	43	14.6	1
APMV_PC_COLOR_125_SCI1	2015-05-05T01:32:05.368	293095437	1678	156	43	14.6	0
APMV_PC_COLOR_128_SCI1	2015-05-08T06:38:05.371	293372997	1601	335	43	14.7	1
APMV_PC_COLOR_129_SCI1	2015-05-09T03:14:05.372	293447157	1581	287	43	14.7	0
APMV_PC_COLOR_129_SCI3	2015-05-09T20:04:05.373	293507757	1564	247	43	14.7	1
APMV_PC_COLOR_130_SCI1	2015-05-10T06:30:05.373	293545317	1553	223	43	14.7	0
APMV_PC_COLOR_131_SCI1	2015-05-11T00:18:05.374	293609397	1536	181	43	14.7	1
APMV_PC_COLOR_131_SCI3	2015-05-11T19:46:05.375	293679477	1517	135	43	14.7	0
APMV_PC_COLOR_132_SCI1	2015-05-12T07:44:05.376	293722557	1505	107	43	14.7	1
APMV_PC_COLOR_133_SCI1	2015-05-13T02:39:05.376	293790657	1486	63	43	14.7	0
APMV_PC_COLOR_133_SCI3	2015-05-13T19:31:35.377	293851407	1469	23	43	14.7	1
APMV_PC_COLOR_134_SCI1	2015-05-14T01:42:05.377	293873637	1463	8	43	14.7	0
APMV_PC_COLOR_134_SCI2	2015-05-14T19:45:05.378	293938617	1445	326	43	14.7	1
APMV_PC_COLOR_149_SCI2	2015-05-29T11:38:05.393	295205397	1096	220	43	14.8	1
APMV_PC_COLOR_149_SCI3	2015-05-29T18:34:05.394	295230357	1089	203	43	14.8	0
APMV_PC_COLOR_150_SCI1	2015-05-30T05:50:05.394	295270917	1078	177	43	14.8	0
APMV_PC_COLOR_151_SCI1	2015-05-31T01:21:05.395	295341177	1058	131	43	14.8	1
APMV_PC_COLOR_151_SCI3	2015-05-31T18:44:05.396	295403757	1041	90	43	14.8	1
APMV_PC_COLOR_152_SCI1	2015-06-01T06:03:05.396	295444497	1030	64	43	14.8	0
APMV_PC_COLOR_153_SCI1	2015-06-02T01:28:05.397	295514397	1011	18	43	14.8	1
APMV_PC_COLOR_153_SCI3	2015-06-02T18:12:05.398	295574637	994	339	43	14.8	0
APMV_PC_COLOR_154_SCI1	2015-06-03T04:28:05.398	295611597	984	315	43	14.8	0
APMV_PC_COLOR_157_SCI1	2015-06-06T01:13:05.401	295859097	916	153	43	14.8	1
APMV_PC_COLOR_159_SCI1	2015-06-08T01:23:05.404	296032497	868	40	43	14.8	1
APMV_PC_COLOR_161_SCI1	2015-06-10T01:17:05.406	296204937	820	288	43	14.9	1
APMV_PC_COLOR_163_SCI1	2015-06-12T01:04:06.408	296376957	773	175	43	14.9	0
APMV_PC_COLOR_167_SCI2	2015-06-16T19:05:06.413	296787417	660	268	43	14.9	0
APMV_PC_COLOR_168_SCI1	2015-06-17T05:55:06.414	296826417	649	242	43	14.9	1
APMV_PC_COLOR_169_SCI2	2015-06-18T19:38:06.415	296962197	611	154	43	14.9	0
APMV_PC_COLOR_170_SCI1	2015-06-19T08:04:06.416	297006957	599	124	43	14.9	1
APMV_PC_COLOR_171_SCI1	2015-06-20T01:00:06.416	297067917	582	85	43	14.9	0
APMV_PC_COLOR_172_SCI1	2015-06-21T05:56:06.418	297172077	554	17	43	14.9	1
APMV_PC_COLOR_173_SCI1	2015-06-22T00:34:06.418	297239157	535	333	43	14.9	0
APMV_PC_COLOR_174_SCI1	2015-06-23T03:11:06.419	297334977	509	270	43	14.9	1
PEMV_01_PC_VISUV_MAP_B_0	2015-06-25T05:03:55.421	297514547	459	153	43	14.96	1
PEMV_01_PC_VISUV_MAP_B_3	2015-06-26T09:59:55.423	297618707	431	85	43	15.0	0
PEMV_01_PC_VISUV_MAP_B_6	2015-06-27T04:58:54.923	297687047	412	41	43	15.0	1
PEMV_01_PC_VISUV_MAP_B_9	2015-06-28T09:26:55.425	297789527	383	334	43	15.0	0
PEMV_01_PC_VISUV_MAP_B_12	2015-06-29T04:21:55.425	297857627	365	289	43	15.0	1
PEMV_01_PC_VISUV_MAP_B_19	2015-07-01T17:19:55.428	298077108	304	146	43	15.0	1
PEMV_01_PC_Multi_Map_A_3	2015-07-02T17:48:45.429	298165238	280	89	43	15.0	0
PEMV_01_PC_Multi_Map_A_5	2015-07-03T04:03:55.430	298202148	270	65	43	15.014763	1
PEMV_01_PC_Multi_Map_A_18	2015-07-07T16:44:45.935	298593398	162	169	43	15.1	1
PEMV_01_PC_Multi_Map_B_2	2015-07-08T09:04:45.935	298652198	146	131	43	15.1	0
PEMV_01_PC_Multi_Map_B_3	2015-07-08T17:06:50.936	298681123	138	112	43	15.	1
PEMV_01_PC_Multi_Map_B_5	2015-07-09T03:41:05.936	298719178	127	87	43	15.1	0

Table 7 continued on next page

Table 7 (*continued*)

	Mid-Time of Observation	MET	Image Scale	Sub-s/c Long.	Sub-s/c Lat.	Solar Phase.	Electronics
	(UTC)		(km/pix)	(Deg E)	(Deg N)	(Deg)	Side
PEMV_01_PC_Multi_Map_B_6	2015-07-09T16:56:05.937	298766878	114	56	43	15.1	1
PEMV_01_PC_Multi_Map_B_8	2015-07-10T08:55:30.937	298824443	98	19	43	15.2	0
PEMV_01_PC_Multi_Map_B_9	2015-07-10T16:52:15.938	298853048	90	0	43	15.2	1
PEMV_02_PC_Multi_Map_B_9	2015-07-10T16:55:05.938	298853218	90	0	43	15.2	1
PEMV_01_PC_Multi_Map_B_11	2015-07-11T03:34:35.938	298891588	80	335	43	15.2	0
PEMV_01_PC_Multi_Map_B_12	2015-07-11T16:46:56.439	298939128	67	304	43	15.3	1
PEMV_02_PC_Multi_Map_B_12	2015-07-11T16:49:46.439	298939298	66	304	43	15.3	1
PEMV_01_PC_Multi_Map_B_14	2015-07-12T08:23:08.440	298995300	51	268	43	15.4	0
PEMV_01_PC_Multi_Map_B_15	2015-07-12T16:53:04.940	299025878	43	248	43	15.4	1
PEMV_01_PC_Multi_Map_B_17	2015-07-13T03:38:06.440	299064598	32	223	43	15.6	0
PEMV_01_PC_Multi_Map_B_18	2015-07-13T07:38:36.941	299079028	28	213	43	15.6	1
PEMV_01_PCNH_Multi_Long_1d1	2015-07-13T14:50:51.941	299104958	21	197	43	15.8	0
PEMV_01_PC_Multi_Long_1d2	2015-07-13T21:08:40.941	299127628	15	182	43	16.1	1
PEMV_01_PC_Color_TimeRes	2015-07-14T02:47:54.441	299147983	9	169	42	16.8	0

C. OUTPUT DATA: HST CONVERTED VALUES

[h]

Table 8. Color Observations of Pluto and Charon

Target	MET	Counts		Flux		Converted Magnitude	
		Red	Blue	Red	Blue	Vegamag	
Pluto	290860857	477.8	99.06	1.02e-11	8.119e-12	15.34	16.34
Pluto	291114237	474.2	95.33	1.016e-11	7.839e-12	15.43	16.44
Pluto	291201837	515.2	97.98	1.111e-11	8.109e-12	15.38	16.43
Pluto	291267597	523.5	106.4	1.117e-11	8.72e-12	15.36	16.37
Pluto	291308097	561.3	117.2	1.201e-11	9.631e-12	15.28	16.27
Pluto	291374037	563.6	111.7	1.208e-11	9.186e-12	15.32	16.34
Pluto	291440517	523.6	102.9	1.118e-11	8.438e-12	15.42	16.45
Pluto	291481197	480	95.33	1.029e-11	7.843e-12	15.52	16.54
Pluto	291547077	525.4	105.2	1.127e-11	8.666e-12	15.44	16.45
Pluto	291608877	541.4	105	1.16e-11	8.636e-12	15.43	16.48
Pluto	291651657	565	111.3	1.213e-11	9.178e-12	15.39	16.42
Pluto	291821817	594.7	117	1.266e-11	9.565e-12	15.4	16.43
Pluto	291999777	606.6	124.1	1.294e-11	1.017e-11	15.41	16.41
Pluto	292233837	642.2	132.5	1.367e-11	1.083e-11	15.42	16.42
Pluto	292406157	754.1	157	1.618e-11	1.293e-11	15.29	16.28
Pluto	292546437	699.8	141.5	1.499e-11	1.164e-11	15.43	16.44
Pluto	292750977	778.1	153.4	1.672e-11	1.265e-11	15.39	16.42
Pluto	292922727	824.6	172.4	1.77e-11	1.421e-11	15.36	16.35
Pluto	293095437	848.1	173.3	1.809e-11	1.42e-11	15.4	16.41
Pluto	293372997	916.2	185.9	1.962e-11	1.529e-11	15.42	16.43
Pluto	293447157	1010	209	2.17e-11	1.723e-11	15.33	16.33
Pluto	293507757	1043	207	2.206e-11	1.681e-11	15.35	16.38
Pluto	293545317	1093	224.9	2.344e-11	1.852e-11	15.29	16.29
Pluto	293609397	1053	213	2.25e-11	1.747e-11	15.36	16.38
Pluto	293679477	1005	193.1	2.153e-11	1.589e-11	15.46	16.51
Pluto	293722557	957.8	193.8	2.055e-11	1.596e-11	15.51	16.52
Pluto	293790657	1064	215.6	2.279e-11	1.773e-11	15.42	16.43

Table 8 *continued on next page*

Table 8 (*continued*)

Target	MET	Counts		Flux ($erg \cdot s^{-1} \cdot cm^{-2} \cdot \text{\AA}^{-1}$)		Converted Magnitude	
		Red	Blue	Red	Blue	F555W	Vegamag
Pluto	293851407	1085	221.9	2.318e-11	1.821e-11	15.42	16.43
Pluto	293873637	1152	226.1	2.457e-11	1.852e-11	15.39	16.42
Pluto	293938617	1134	221.8	2.411e-11	1.81e-11	15.43	16.47
Pluto	295205397	2099	414.7	4.486e-11	3.403e-11	15.36	16.38
Pluto	295230357	2201	442.5	4.696e-11	3.625e-11	15.31	16.33
Pluto	295270917	2161	441	4.602e-11	3.605e-11	15.35	16.36
Pluto	295341177	2010	385	4.275e-11	3.144e-11	15.5	16.55
Pluto	295403757	2081	406.7	4.457e-11	3.345e-11	15.48	16.51
Pluto	295444497	2223	439.2	4.787e-11	3.631e-11	15.42	16.45
Pluto	295514397	2347	428.5	5.053e-11	3.542e-11	15.43	16.52
Pluto	295574637	2478	500.5	5.302e-11	4.111e-11	15.38	16.39
Pluto	295611597	2553	504.4	5.442e-11	4.128e-11	15.38	16.41
Pluto	295859097	2672	519.4	5.722e-11	4.271e-11	15.49	16.53
Pluto	296032497	3088	607.5	6.663e-11	5.034e-11	15.43	16.47
Pluto	296204937	3613	720.3	7.716e-11	5.907e-11	15.39	16.41
Pluto	296376957	4216	840.9	9.01e-11	6.899e-11	15.35	16.38
Pluto	296787417	5868	1162	1.254e-10	9.538e-11	15.34	16.37
Pluto	296826417	6021	1204	1.296e-10	9.958e-11	15.34	16.36
Pluto	296962197	6444	1292	1.374e-10	1.058e-10	15.4	16.42
Pluto	297006957	6153	1206	1.321e-10	9.942e-11	15.5	16.53
Pluto	297067917	6838	1341	1.454e-10	1.095e-10	15.45	16.49
Pluto	297172077	7671	1512	1.652e-10	1.25e-10	15.42	16.45
Pluto	297239157	8519	1681	1.829e-10	1.386e-10	15.39	16.42
Pluto	297334977	9512	1887	2.037e-10	1.552e-10	15.38	16.4
Pluto	297687047	1.361e+04	2692	2.914e-10	2.214e-10	15.45	16.48
Pluto	297789527	1.648e+04	3237	3.522e-10	2.656e-10	15.4	16.43
Pluto	297857627	1.782e+04	3568	3.838e-10	2.95e-10	15.41	16.43
Pluto	298077108	2.465e+04	4957	5.259e-10	4.061e-10	15.46	16.47
Pluto	298165238	2.871e+04	5669	6.159e-10	4.669e-10	15.47	16.5
Charon	290860857	69.59	18.64	1.488e-12	1.553e-12	17.3	17.96
Charon	291114237	56.34	13.96	1.208e-12	1.167e-12	17.63	18.33
Charon	291201837	61.05	15.34	1.318e-12	1.291e-12	17.55	18.25
Charon	291267597	67.63	15.24	1.445e-12	1.269e-12	17.51	18.28
Charon	291308097	65.76	19.67	1.409e-12	1.643e-12	17.43	18.01
Charon	291374037	72.55	21.36	1.557e-12	1.787e-12	17.35	17.94
Charon	291440517	70.33	14.58	1.504e-12	1.215e-12	17.55	18.38
Charon	291481197	65.56	15.58	1.407e-12	1.304e-12	17.58	18.31
Charon	291547077	70.49	20.64	1.515e-12	1.728e-12	17.43	18.03
Charon	291608877	69.18	14.96	1.485e-12	1.252e-12	17.59	18.39
Charon	291651657	73.51	16.9	1.581e-12	1.417e-12	17.51	18.27
Charon	291821817	69.51	18.69	1.482e-12	1.553e-12	17.57	18.22
Charon	291999777	85.95	19.86	1.837e-12	1.654e-12	17.45	18.21
Charon	292233837	78.03	23.85	1.664e-12	1.982e-12	17.51	18.08
Charon	292406157	91.1	23.78	1.957e-12	1.991e-12	17.46	18.13
Charon	292546437	94.57	21.6	2.029e-12	1.806e-12	17.52	18.28
Charon	292750977	92	26.18	1.98e-12	2.196e-12	17.52	18.14
Charon	292922727	94.54	17.49	2.032e-12	1.465e-12	17.72	18.64
Charon	293095437	117	27.59	2.5e-12	2.299e-12	17.47	18.21
Charon	293372997	117.5	25.06	2.521e-12	2.096e-12	17.6	18.41
Charon	293447157	129	32.49	2.774e-12	2.724e-12	17.46	18.15
Charon	293507757	125.8	28.84	2.665e-12	2.382e-12	17.56	18.32
Charon	293545317	135	31.5	2.9e-12	2.639e-12	17.48	18.22

Table 8 continued on next page

Table 8 (*continued*)

Target	MET	Counts		Flux ($erg \cdot s^{-1} \cdot cm^{-2} \cdot \text{\AA}^{-1}$)		Converted Magnitude	
		Red	Blue	Red	Blue	F555W	F435W
Charon	293609397	126.1	35.81	2.697e-12	2.986e-12	17.5	18.12
Charon	293679477	137.7	30	2.955e-12	2.51e-12	17.54	18.33
Charon	293722557	130.8	28.7	2.811e-12	2.404e-12	17.61	18.4
Charon	293790657	130.4	32.02	2.797e-12	2.678e-12	17.59	18.31
Charon	293851407	131.7	26.69	2.818e-12	2.227e-12	17.69	18.53
Charon	293873637	140.1	37.84	2.995e-12	3.152e-12	17.51	18.16
Charon	293938617	150.3	28.51	3.2e-12	2.366e-12	17.61	18.5
Charon	295205397	247.2	53.47	5.291e-12	4.461e-12	17.61	18.41
Charon	295230357	273	61.64	5.834e-12	5.135e-12	17.5	18.27
Charon	295270917	279.2	64.82	5.954e-12	5.388e-12	17.49	18.24
Charon	295341177	268.7	58.68	5.724e-12	4.873e-12	17.6	18.39
Charon	295403757	283.4	60.3	6.08e-12	5.042e-12	17.58	18.39
Charon	295444497	279.5	72.67	6.027e-12	6.11e-12	17.53	18.2
Charon	295514397	284.7	75.38	6.141e-12	6.337e-12	17.54	18.21
Charon	295574637	299.1	68.1	6.41e-12	5.688e-12	17.6	18.36
Charon	295611597	311	78.22	6.639e-12	6.509e-12	17.54	18.24
Charon	295859097	350.8	80.25	7.526e-12	6.71e-12	17.6	18.36
Charon	296032497	385.4	90.47	8.33e-12	7.623e-12	17.59	18.34
Charon	296204937	446.4	110.2	9.55e-12	9.19e-12	17.55	18.26
Charon	296376957	552.5	125.5	1.183e-11	1.047e-11	17.48	18.24
Charon	296787417	722.1	171.2	1.546e-11	1.429e-11	17.51	18.25
Charon	296826417	747.7	174.8	1.613e-11	1.47e-11	17.51	18.25
Charon	296962197	853.7	202.7	1.823e-11	1.688e-11	17.5	18.23
Charon	297006957	844.7	187.6	1.817e-11	1.573e-11	17.57	18.35
Charon	297067917	916.1	211.5	1.951e-11	1.756e-11	17.54	18.3
Charon	297172077	954.5	217.2	2.059e-11	1.826e-11	17.6	18.36
Charon	297239157	1067	249.2	2.296e-11	2.089e-11	17.54	18.29
Charon	297334977	1181	277.1	2.534e-11	2.317e-11	17.55	18.29
Charon	297687047	1694	380.7	3.635e-11	3.183e-11	17.63	18.4
Charon	297789527	2054	481	4.397e-11	4.013e-11	17.56	18.31
Charon	297857627	2281	531.1	4.92e-11	4.465e-11	17.55	18.3
Charon	298077108	3322	777	7.1e-11	6.473e-11	17.54	18.29
Charon	298165238	3924	907.3	8.43e-11	7.599e-11	17.54	18.3